Ciliated sensory hair cell formation and function require the F-BAR protein syndapin I and the WH2 domain-based actin nucleator Cobl

Susann Schüler, Judith Hauptmann, Birgit Perner, Michael M. Kessels, Christoph Englert and Britta Qualmann

Journal of Cell Science 126, 4059

doi: 10.1242/jcs.138917

There was an error published in *J. Cell Sci.* **126**, 196-208.

The sequence of MO sdpI_e3i3 was reported incorrectly in the Materials and Methods section. The correct sequence of the MO sdpI_e3i3 used for this study is gtcaaaatccttcctcacCTCTCTC.

We apologise for this mistake.

Ciliated sensory hair cell formation and function require the F-BAR protein syndapin I and the WH2 domain-based actin nucleator Cobl

Susann Schüler[1], Judith Hauptmann[1,*], Birgit Perner[2], Michael M. Kessels[1,‡], Christoph Englert[2,‡] and Britta Qualmann[1,‡]

[1]Institute of Biochemistry I, Jena University Hospital/Friedrich-Schiller-University Jena, 07743 Jena, Germany
[2]Department of Molecular Genetics, Leibniz Institute for Age Research/FLI, 07745 Jena, Germany

*Present address: Department of Biochemistry, University Regensburg, 93053 Regensburg, Germany
‡Authors for correspondence (michael.kessels@mti.uni-jena.de; cenglert@fli-leibniz.de; britta.qualmann@mti.uni-jena.de).

Accepted 19 November 2012
Journal of Cell Science 126, 196–208

doi: 10.1242/jcs.111674

Summary

During development, general body plan information must be translated into distinct morphologies of individual cells. Shaping cells is thought to involve cortical cytoskeletal components and Bin-Amphiphysin-Rvs167 (BAR) superfamily proteins. We therefore conducted comprehensive side-by-side loss-of-function studies of zebrafish orthologs of the F-BAR protein syndapin I and the actin nucleator Cobl. Zebrafish syndapin I associates with Cobl. The loss-of-function phenotypes of these proteins were remarkably similar and suggested a common function. Both *cobl*- and *syndapin I*-morphant fish showed severe swimming and balance-keeping defects, reflecting an impaired organization and function of the lateral line organ. Their lateral line organs lacked several neuromasts and showed an impaired functionality of the sensory hair cells within the neuromasts. Scanning electron microscopy revealed that sensory hair cells of both *cobl*- and *syndapin I*-morphant animals showed defects in the formation of both microtubule-dependent kinocilia and F-actin-rich stereocilia. Consistent with the kinocilia defects in sensory hair cells, body length was shortened and the development of body laterality, a process depending on motile cilia, was also impaired. Interestingly, Cobl and syndapin I both localized to the base of forming cilia. Rescue experiments demonstrated that proper formation of ciliated sensory hair cell rosettes relied on Cobl's syndapin I-binding Cobl homology domain, the actin-nucleating C-terminus of Cobl and the membrane curvature-inducing F-BAR domain of syndapin I. Our data thus suggest that the formation of distinct types of ciliary structures relies on membrane topology-modulating mechanisms that are based on F-BAR domain functions and on complex formation of syndapin I with the actin nucleator Cobl.

Key words: WH2 domain-based actin nucleator cordon-bleu, PACSIN, Lateral line organ, Kinocilia and Stereocilia, Ciliogenesis

Introduction

During development of multicellular organisms, general body plan information, i.e. definition of body axes and pattern formation, has to be translated into distinct morphologies of individual cells. On the cellular level, two types of polarization can be distinguished: apical–basal polarity, a process, e.g. crucial for epithelia formation and neuromorphogenesis, and planar cell polarity, during which cells polarize orthogonally to epithelial cell layers (St Johnston and Sanson, 2011), a process, e.g. observed during development of sensory hair cells in the inner ear and in the neuromasts of the teleost lateral line, organs crucial for orientation and balance keeping (Ma and Raible, 2009).

Little is known about the actual molecular effectors bringing about the required cell shape changes during polarity establishment and maintenance. Mechanisms of membrane shaping include protein insertion and imprinting shapes of membrane-binding proteins onto membranes (scaffolding) (Qualmann et al., 2011; McMahon and Gallop, 2005) as well as force generation by the cortical actin cytoskeleton. Cobl/syndapin I complexes seem to combine these different mechanisms: Syndapin I is a lipid-binding and membrane curvature-sensing spatial organizer (Qualmann and Kelly, 2000; Kessels and Qualmann, 2006; Dharmalingam et al., 2009; Itoh et al., 2005). *Syndapin I* knockout mice suffer from seizures and show deficits in membrane anchoring of dynamin (Koch et al., 2011). Additionally, syndapin I associates with and recruits the actin nucleator Cobl to the cortex of neurons (Schwintzer et al., 2011).

Cobl uses three Wiskott-Aldrich homology 2 (WH2) domains for actin-binding and nucleation (Ahuja et al., 2007). *In vitro*-experiments with C-terminal fragments of human Cobl suggested that Cobl may additionally increase the number of barbed ends by severing filaments (Husson et al., 2011). Cobl induced F-actin-rich membrane ruffles in COS-7 cells and excessive dendrite formation and branching in neurons and knock-down studies demonstrated that Cobl is critical for dendritogenesis of dissociated hippocampal neurons and of cerebellar Purkinje cells (Ahuja et al., 2007; Haag et al., 2012).

Cobl is predominantly expressed in the nervous system (Ahuja et al., 2007). During early development of mice, *Cobl* mRNA was also found in the early organizer node suggesting a putative role in pattern formation. The original *Cobl* gene trap allele, however, is a weak hypomorph (Gasca et al., 1995; Carroll et al., 2003) and thus not suitable to test *Cobl* functions in vertebrate development.

The zebrafish is a powerful model organism for functional and developmental studies. We therefore cloned zebrafish *cobl* and *syndapin I*, verified their interaction and analyzed *cobl* and *syndapin I* loss-of-function phenotypes at the cellular, organ, whole-animal and behavioral level. Our data show that lack of Cobl and syndapin I results in similar loss-of-function phenotypes in developmental and behavioral processes that rely on proper formation and function of motile and non-motile sensory cilia, kinocilia and/or stereocilia. The observed localization of both syndapin I and Cobl at the base of forming cilia and the functional domain requirements revealed in rescue experiments at the whole animal level suggest that membrane topology modulation by combining actin cytoskeletal and direct membrane shaping functions of Cobl/syndapin I complexes are crucial for formation of ciliary structures.

Results

Danio rerio Cobl and syndapin I

Database analyses identified a single gene (JQ776648) encoding a *Danio rerio* ortholog of Cobl. An N-terminal Cobl homology domain and a cluster of three C-terminal WH2 domains clearly identified JQ776648 as ortholog of mammalian Cobl (Fig. 1A; supplementary material Fig. S1).

Mammalia have three syndapins (also called PACSINs) (Kessels and Qualmann, 2004). In line with teleost fish-specific genome duplication (Hoegg et al., 2004), our analyses showed that zebrafish has six genes encoding syndapins. Detailed phylogenetic analyses revealed that *Danio rerio* syndapin I/PACSIN1b (ENSDART00000128456) resembles mammalian syndapin I [supplementary material Fig. S2; also see Edeling et al. (Edeling et al., 2009)].

Using cDNA from 24 hours post fertilization (hpf) we cloned full-length zebrafish *cobl* and deletion mutants, and full-length *syndapin I* and its SH3 domain (Fig. 1A,B; supplementary material Figs S1, S2). Affinity-purification experiments with immobilized syndapin I (data not shown) and with its SH3 domain showed that zebrafish syndapin I associates with zebrafish Cobl (Fig. 1C). Thus, syndapin I interaction appears to be an important aspect of Cobl function in both fish and mammals.

Further experiments revealed that syndapin association occurred with the N-terminal Cobl homology domain but not with the Cobl C-terminus (Fig. 1C). This is in line with three KrrAPpPP motifs – representing syndapin binding sites in mammals (Schwintzer et al., 2011) – being highly conserved among mouse, human, chicken, frog and zebrafish Cobl (supplementary material Fig. S1).

Gene expression analyses at different developmental stages showed that both *cobl* and *syndapin I* are maternally expressed. *Cobl* mRNA levels were relatively low during the first 24 hpf and increased between 24 and 48 hpf. After a maximum at 48 hpf, levels remained relatively constant up to 5 days post fertilization (dpf). In contrast, *syndapin I* mRNA was already present at high levels at fertilization and remained high (Fig. 1D).

In situ hybridizations revealed that both *cobl* and *syndapin I* are largely restricted to neuronal tissue, such as forebrain, hindbrain, midbrain–hindbrain boundary, spinal cord and retina (Fig. 1E–J). At 24 hpf, *cobl* expression was additionally observed in somites (Fig. 1E) and the pronephric duct (Fig. 1E, arrowhead). Corresponding sense probes did not lead to any staining (data not shown). This suggested that the *cobl* and *syndapin I* detections were specific.

Knock-down of *cobl* and *syndapin I* leads to similar defects in brain, body and motile cilia-driven body laterality development

We next designed morpholino oligonucleotides (MO) against *cobl* and *syndapin I* to analyze and compare putative *cobl* and *syndapin I* loss-of-function phenotypes. MO *syndapin I*(*sdpI*)_ATG targets translation. Three further MOs were designed to suppress proper splicing of *cobl* and *syndapin I* mRNAs (Fig. 2A,B). MO effectiveness was tested via RT-PCR on cDNA isolated from injected embryos. All splice-morpholinos, MO *cobl*_i3e4, MO *cobl*_e4i4 and MO *sdpI*_e3i3, led to strong and dose-dependent decreases of *cobl* and *syndapin I* mRNA levels, respectively. In the case of MO *cobl*_e4i4, 0.1 and 0.2 pmol were not as effective (results not shown), and higher doses were needed for comparable knock-down (Fig. 2C,D). Phenotypical comparisons (see below) suggested that MO *sdpI_ATG* injection also effectively and specifically knocked down *syndapin I*.

Cobl MO-injected embryos showed that embryos at 24 hpf displayed a shortened anterior–posterior body axis, a curved body shape, smaller heads and eyes as well as oedema in heart and brain (Fig. 2E). Compared to wild-type or control-injected individuals, 48 hpf embryos additionally showed considerably enlarged brain ventricles (Fig. 2H,I).

Syndapin I-deficient embryos had smaller heads and eyes than control embryos. Their bodies were curved and, at higher doses, such as 0.4 pmol, they had a shortened body axis. Oedema in heart and brain occurred at 24 hpf as well as at 48 hpf. Enlarged ventricles indicate an impaired brain development (Fig. 2F,G,I,J). *Syndapin I* morphants thus closely phenocopied *cobl* loss-of-function. The similarity of the phenotypes is also reflected by quantitative analyses of body length (Fig. 2K).

In all cases, the phenotypes were dose-dependent and not caused by the injection procedure itself, as confirmed by control injections (data not shown). Importantly, the phenotypes were consistent between MO *cobl*_i3e4- and MO *cobl*_e4i4-injected embryos (Fig. 2E) and between MO *sdpI*_ATG- and MO *sdpI*_e3i3-injected embryos (Fig. 2G), respectively.

Double-knock-down of *cobl* and *syndapin I*, even at low doses (e.g. 0.2 pmol MO *cobl*_i3e4 and 0.4 pmol MO *sdpI*_ATG) led to dramatically enhanced phenotypes. Morphants displayed strongly shortened anterior–posterior body axes, oedemas and impaired somitogenesis. The brain was much more unstructured and displayed strong necrotic defects (Fig. 2L,M).

mRNA distribution in mice suggested that Cobl may be involved in axis formation (Gasca et al., 1995). We therefore analyzed *cobl* MO-injected embryos for laterality defects using *pitx2,* a lateral plate mesoderm marker. At 20–22 somite stages, induced by signals from Kupffer's vesicle (Lopes et al., 2010), *pitx2* mRNA is exclusively expressed at the left body side of wild-type (Fig. 2N, left panel, arrowhead) and control-injected embryos (*p53*) (Fig. 2O).

In contrast, *cobl* MO-injected embryos showed impaired laterality formation. Only 45% of MO *cobl*_i3e4-injected embryos showed correct *pitx2* expression on the left, whereas 6% showed *pitx2* on the right and 1.5% on both sides. Such defects were never observed in uninjected or control-injected embryos. Furthermore, about 45% of all MO *cobl*_i3e4-injected embryos lacked *pitx2* expression at either side (Fig. 2N,O).

Knock-down of *syndapin I* also resulted in strong laterality defects. Only about 45% of embryos injected with MO

*sdpI*_ATG or MO *sdpI*_e3i3 showed correct *pitx2* expression at the left body side. 7% (MO *sdpI*_ATG) and 19% (MO *sdpI*_e3i3) of the embryos showed expression at the opposite side, while 14% (MO *sdpI*_ATG) and 33% (MO *sdpI*_e3i3) showed bilateral *pitx2* expression (Fig. 2N,O). Thus, similar laterality defects were observed in *cobl* and *syndapin I* morphants.

Both *cobl* and *syndapin I* morphants show circular movements and defects in balance keeping

Both *cobl* and *syndapin I* morphants exhibited alterations in swimming behavior. We therefore analyzed behavioral phenotypes in detail. As neither *cobl* nor *syndapin I* morphants hatched by themselves (not shown), all larvae, including control animals, were dechorionated prior to experiments. At 48 hpf, uninjected (not shown) and control-injected larvae displayed C-bend behaviors and fast and directed escape reactions upon tactile stimulation (Fig. 3A; supplementary material Movie 1). In contrast, the majority of both *cobl* and *syndapin I* morphants did not respond but remained largely immotile. The minority of *cobl* and *syndapin I* morphants that did move displayed behavioral phenotypes: They failed to show a directed escape but displayed uncoordinated and circular movements (Fig. 3B–D).

Whereas all control animals were properly orientated upright; more than 70% of the morphants were unable to keep their balance and lay on their sides (Fig. 3A–C,E; supplementary material Movies 1–3).

Cobl and *syndapin I* morphants show defects in posterior lateral line organization

In mammals, balance keeping and coordination in space is predominantly an inner ear function. In fish, the anterior and the posterior lateral lines, regular arrays of neuromast rosettes, have similar functions (Haas and Gilmour, 2006; Ma and Raible, 2009). *Cobl* and *syndapin I* expression was enriched in discrete spots along the tail of fish (Fig. 4A,B). *In situ* hybridization of the lateral line marker *eya1* (Sahly et al., 1999) showed a similar, regular pattern of spots along the tail (Fig. 4C, arrowheads).

MO *cobl*_i3e4 (0.2 pmol) and MO *cobl*_e4i4 (0.6 pmol) injection both consistently led to fewer *eya1*-positive neuromasts compared to control-injected fish. Similarly, *syndapin I* knock-down by either MO *sdpI*_ATG (0.4 pmol) or MO *sdpI*_e3i3 (0.3 pmol) led to a reduction of neuromasts (Fig. 4C–H).

MO *p53-c*ontrol experiments showed that the observed impairments were not predominantly caused by *p53*-dependent apoptotic processes but specifically represented *cobl* and *syndapin I* loss-of-function phenotypes (Fig. 4H).

Neuromasts of the posterior lateral line organ in *cobl* and *syndapin I* morphants are polarized and innervated, but not functional

The use of phalloidin (supplementary material Fig. S3) and of a transgenic *claudinB:lyn(GFP)* line (Haas and Gilmour, 2006) showed that the fewer neuromast rosettes that still were formed in *cobl*- and *syndapin I*-morphant larvae appeared relatively normal in organization (Fig. 5A,D,G,J).

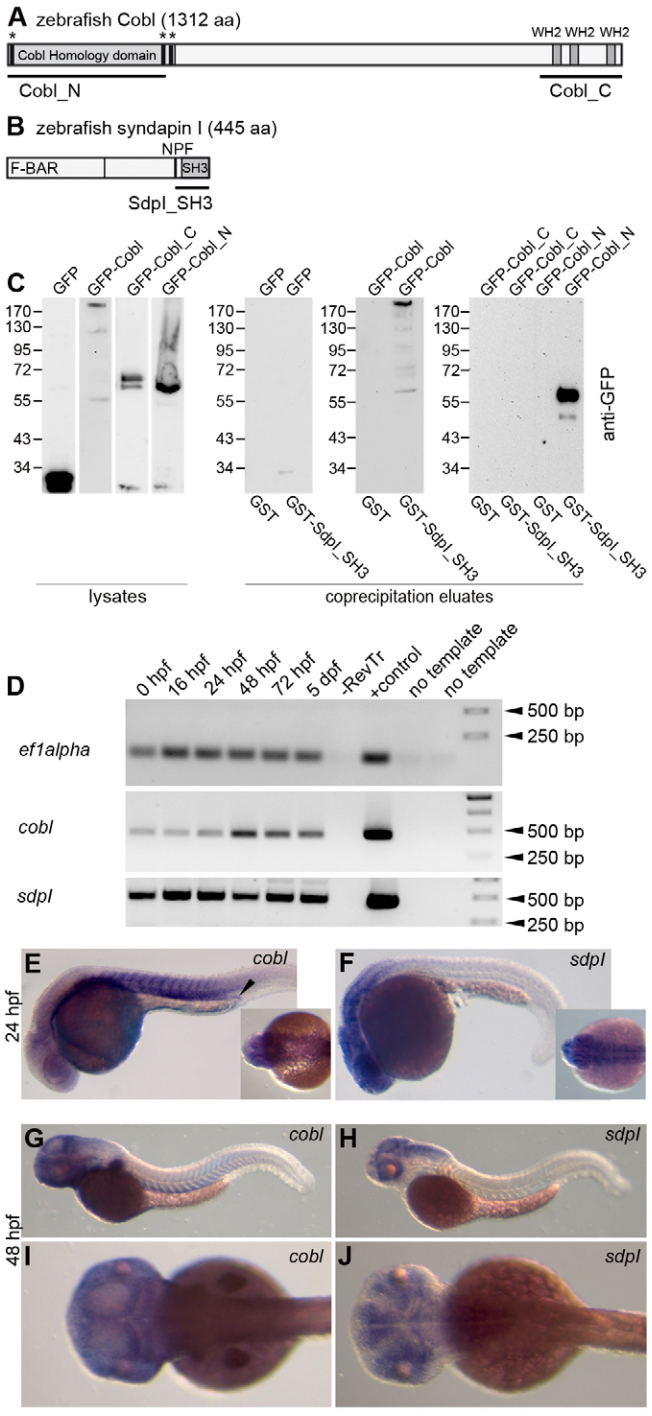

Fig. 1. Biochemical interaction and expression of zebrafish Cobl and syndapin I. (**A**) Domain structure of zebrafish Cobl (JQ776648) with Cobl homology domain, three KrRAPpPP motifs (asterisks) and three WH2 domains. Black lines represent deletion mutants used in the present study. (**B**) Domain structure of zebrafish syndapin I and a deletion mutant used. NPF, Asn-Pro-Phe motif. (**C**) Co-precipitation experiments with zebrafish Cobl and N- and C-terminal fragments thereof (Cobl_N, Cobl_C) expressed as GFP-fusion proteins and immobilized, recombinant GST-syndapin I SH3 domain (GST-SdpI_SH3) and GST, respectively, analyzed by anti-GFP immunoblotting of cell lysates (input) and eluates. (**D**) Expression levels of *cobl* and *syndapin I* (*sdpI*) at 0 hpf to 5 dpf analyzed by RT-PCR. –RevTr, without reverse transcriptase. (**E–J**) Tissue-specific expression patterns of *cobl* (E,G,I) and *syndapin I* (F,H,J) analyzed by *in situ* hybridization at 24 hpf (E, F) and 48 hpf (G–J). Insets in E and F show dorsal head views. *Cobl* and *syndapin I* are expressed in neuronal tissues. *Cobl* expression was additionally detected in somites (especially at 24 hpf; E) and the pronephros (arrowhead in E).

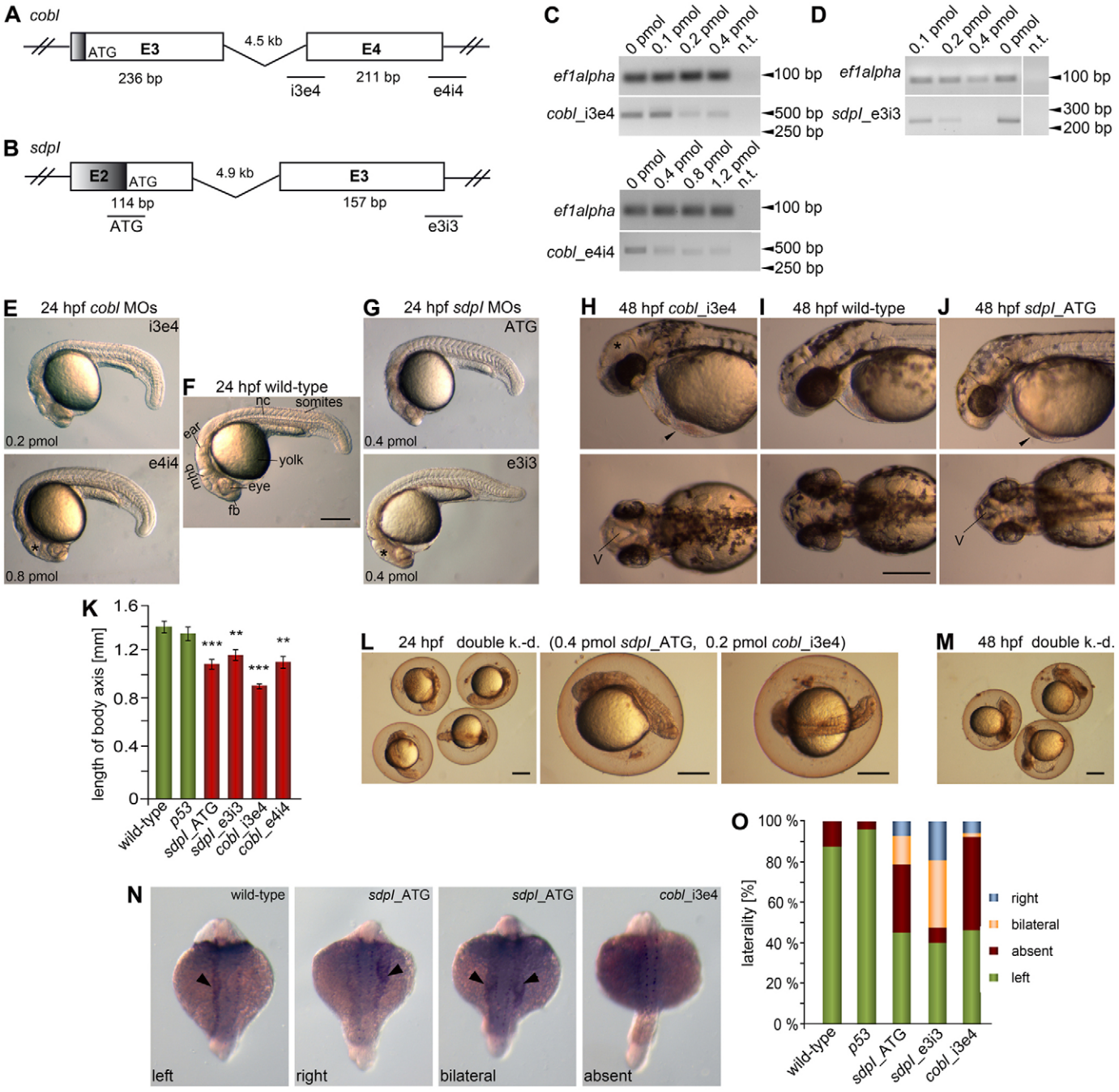

Fig. 2. MO-mediated knock-down of *cobl* and *syndapin I* leads to similar defects in brain, body and motile cilia-driven body laterality development. (**A**,**B**) Position of MOs for *cobl* (A) and *syndapin I* (B) on the respective genes (ORF in white; UTRs in grey). MO *cobl*_i3e4 and MO *cobl*_e4i4 prevent correct splicing (A). For *syndapin I*, an ATG-targeting and a splice-preventing MO (*sdpl*_e3i3) were designed (B). (**C**,**D**) Knock-down of *cobl* (C) and *syndapin I* (D) using increasing amounts of the splice-preventing MOs *cobl*_i3e4, *cobl*_e4i4 and *sdpl*_e3i3 validated via RT-PCR using whole-body mRNA at 24 h post injection and at the 16 somite stage for MO *cobl*_i3e4; *ef1alpha* amplification was used for normalization. n.t., no template. (**E**–**J**) *Cobl*- and *syndapin I*-morphant embryos show similar phenotypes at 24 hpf (E,G) and 48 hpf (H,J). Note the shortened anterior–posterior body axes, heart (arrowheads) and brain with oedema (asterisks) and increased ventricle sizes (examples marked), and smaller heads and eyes. (**L**,**M**) Double knock-down of *cobl* and *syndapin I* leads to dramatically enhanced phenotypes (L, 24 hpf; M, 48 hpf) (embryos not dechorionated). Scale bars: 250 µm. fb, forebrain; mhb, midbrain-hindbrain boundary; nc, notochord; v, ventricle. (**K**) Quantitative analysis of lengths of the body axis at 24 hpf. Wild-type, $n=18$; MO *p53*, $n=9$; MO *sdpl*_ATG, $n=12$; MO *sdpl*_e3i3, $n=15$; MO *cobl*_i3e4, $n=20$; MO *cobl*_e4i4, $n=7$. Statistical analyses, ANOVA with Tukey's test versus wild-type. $^{**}P<0.01$, $^{***}P<0.001$. (**N**,**O**) *Cobl* and *syndapin I* morphants display impaired laterality formation (*in situ* hybridization of *pitx2* (arrowheads); exemplary images underscoring quantification of *pitx2* distribution in wild-type, control-injected (*p53*) and morphant embryos at 20–22 somite stages). Wild-type, $n=174$; MO *p53*, $n=47$; MO *sdpl*_ATG, $n=42$; MO *sdpl*_e3i3, $n=42$; MO *cobl*_i3e4, $n=67$.

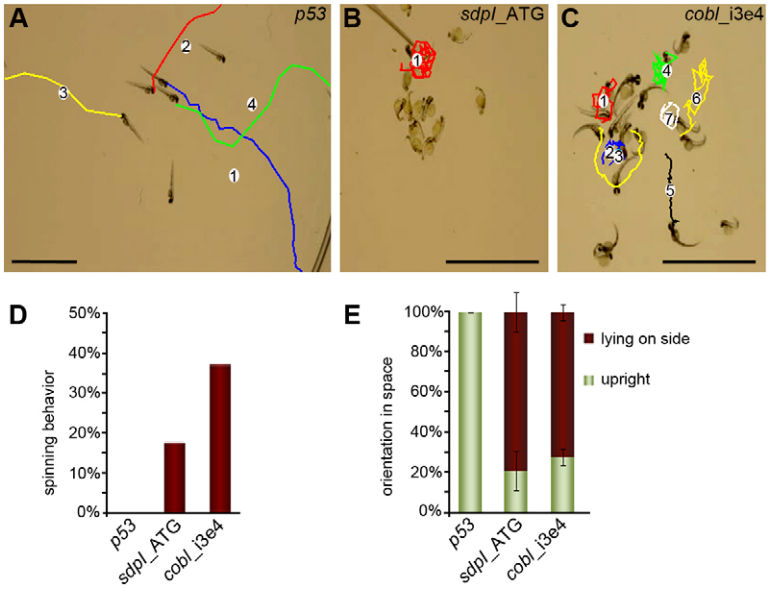

Fig. 3. *Cobl* and *syndapin I* morphants are paralyzed or display uncoordinated movements and fail to keep their balance. (**A–C**) Dechorionated control-injected embryos (48 hpf) show typical directed escape responses after tactile stimulation (A), whereas *syndapin I* (B) and *cobl* (C) morphants did not respond or moved in an uncoordinated spinning manner. The swim paths of moving fish (numbered) are depicted. Note that both *cobl*- and *syndapin I*-morphant fish also often lie on their side. Scale bars: 5 mm. (**D**) Quantification of the percentage of fish showing uncoordinated spinning behavior [control-injected (MO *p53*), $n=28$; MO *sdpl*_ATG, $n=18$; MO *cobl*_i3e4, $n=77$ animals]. (**E**) Quantitative analysis of balance keeping after tactile stimulation. *SdpI*- and *cobl*-morphant embryos lie on their sides and fail to orientate upright (MO *p53*, $n=10$; MO *sdpl*_ATG, $n=40$; MO *cobl*_i3e4, $n=24$; two independent experiments at 48 hpf).

Neuromast rosettes contain central hair cells as sensory units (Haas and Gilmour, 2006; Ma and Raible, 2009). Anti-acetylated-tubulin immunolabeling showed that all rosettes were contacted by axons (supplementary material Fig. S3).

Several vital dyes selectively label neuromast sensory hair cells when their mechanotransduction channels are activated (Santos et al., 2006). Confocal microscopy confirmed that wild-type and *p53*-control MO-injected 4 dpf-larvae internalized FM 4-64FX (Fig. 5B,E). In contrast, both *cobl* MO- and *syndapin I* MO-injected larvae did not show any FM 4-64FX internalization (Fig. 5H,K). Thus, the mechanosensory hair cells of *cobl*- and *syndapin I*-deficient animals were insensitive to sensory inputs.

Both F-actin-rich stereocilia and microtubule-based kinocilia of sensory hair cells of posterior lateral line neuromasts are defective in *cobl* and *sdpl* morphants

Putative degenerative effects could contribute to the functional defects observed in relatively mature neuromasts (4 dpf) (Fig. 5). We therefore next analyzed the sensory apparatus of the posterior lateral line early during its development, at 72 hpf. Each sensory hair cell in a neuromasts rosette apically shows one microtubule-based kinocilium and several small actin-rich stereocilia as sensory apparatus. Scanning electron microscopy (SEM) showed that neuromast rosettes of wild-type animals had 6–8 long, usually bundled, central kinocilia and many much shorter and thinner stereocilia surrounding them (Fig. 6A).

In *cobl* and *syndapin I* morphants, the fewer neuromasts that still were recognizable showed dramatic defects. Both kinocilia and stereocilia were significantly shortened when compared to control animals (Fig. 6A–D). Quantitative experiments with embryos of identical age demonstrated that the effects of *cobl*- and *syndapin I*-deficiency were strong and in many cases highly statistically significant (Fig. 6E,F). This was despite the underestimation caused by our decision to include only clearly recognizable, i.e. the least affected, neuromasts and clearly recognizable and distinguishable ciliary structures in the quantitative analyses. Stereocilia found in *sdpl*_e3i3-morphant neuromasts were shortened by 24% and by about 50% in both *sdpl*_ATG and *cobl*_i3e4 morphants when compared to control-injected fish (Fig. 6E).

The fewer kinocilia that were still formed in *syndapin I*- and *cobl*-deficient fish were also shortened to about 50% of control values (Fig. 6A–D,F). Thus, shaping the apical ciliated compartment of sensory hair cells critically relies on the actin nucleator Cobl and its physical interaction partner syndapin I.

Syndapin I and Cobl localize to forming cilia

The crucial role of syndapin I and Cobl in neuromast development suggested that both proteins may be important effectors in early ciliogenesis. We thus induced primary cilia in embryonic zebrafish cells (ZF4 cells) and visualized GFP-tagged syndapin I 24 h later. In contrast to GFP, GFP-syndapin I specifically accumulated at newly forming cilia highlighted by anti-acetylated-tubulin immunolabeling. The N-terminus of Cobl (GFP-Cobl_N) localized to cilia similar to syndapin I. GFP-Cobl was hardly expressible but, in the few transfected cells obtained, also full-length Cobl and syndapin I co-localized at cilia (Fig. 7A–M).

Interestingly, both syndapin I and Cobl did not localize to the entire length of the forming cilia protruding from the cell surface but often were restricted to areas of varying extension located in the plane of the plasma membrane (Fig. 7D–M).

We next purified mRNA from ZF4 cells and analyzed *syndapin I* and *cobl* expression. RT-PCR with *cobl*-specific primers yielded a faint band of correct size, as confirmed by a *cobl*-plasmid control. *Syndapin I* was also detected in ZF4 cells (Fig. 7N). Thus, ZF4 cells may theoretically also enable localization studies of endogenous proteins, in particular of the more readily detectable syndapin I.

We next affinity-purified antibodies originally raised against mammalian syndapin I (Qualmann et al., 1999) with zebrafish fusion proteins. Western blotting of extracts of HEK293 cells transfected with GFP-syndapin I showed that the affinity-purified antibodies indeed recognized zebrafish syndapin I (Fig. 7O).

Anti-syndapin I immunolabeling of ZF4 cells 5 h after the induction of cilia formation showed that endogenous syndapin I

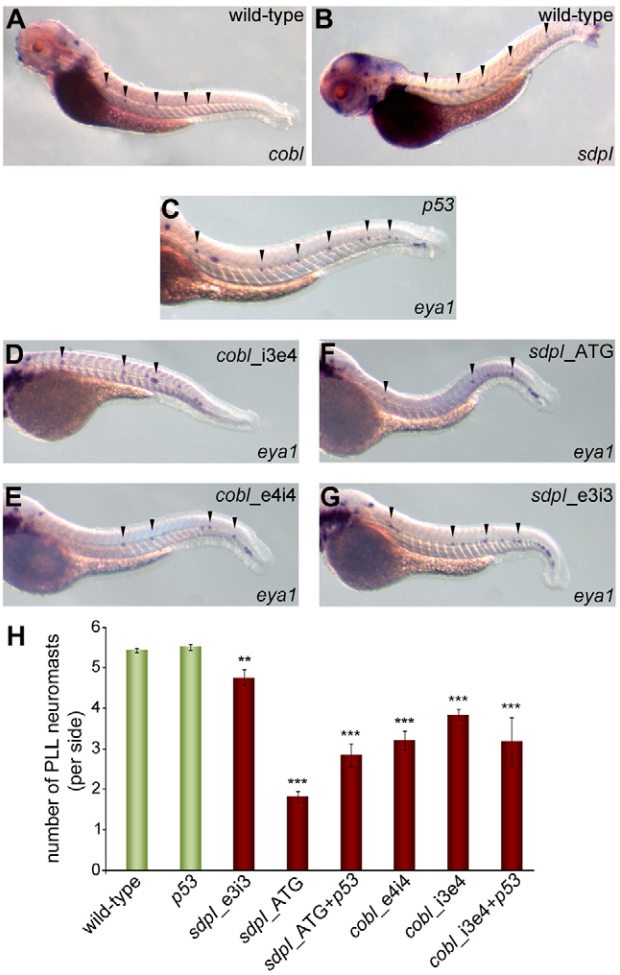

Fig. 4. Knock-down of either *cobl* or *syndapin I* diminishes neuromasts of the posterior lateral line organ. (**A**,**B**) Wild-type zebrafish (72 hpf) analyzed for *cobl* and *syndapin I* expression patterns by *in situ* hybridization. Arrowheads mark regular arrays of *cobl*- and *syndapin I*-positive spots in the tails. (**C**–**G**) *In situ* hybridization of *eya*1 (neuromast marker) at 48 hpf. Neuromasts at the facing tail side are marked by arrowheads. (D–G) Knock-down of *cobl* (D,E) and *syndapin I* (F,G) leads to reduced neuromast numbers. (**H**) Quantitative analysis. Wild-type, $n=117$; MO *p53*, $n=55$; MO *sdpl*_e3i3, $n=27$; MO *sdpl*_ATG, $n=58$; MOs *sdpl*_ATG+*p53*, $n=17$; MO *cobl*_e4i4, $n=16$; MO *cobl*_i3e4, $n=48$; MOs *cobl*_i3e4+*p53*, $n=26$. ANOVA with Tukey's test versus MO *p53*; $^{**}P<0.01$ for MO *sdpl*_e3i3 and $^{***}P<0.001$ for all other data sets. PLL, posterior lateral line.

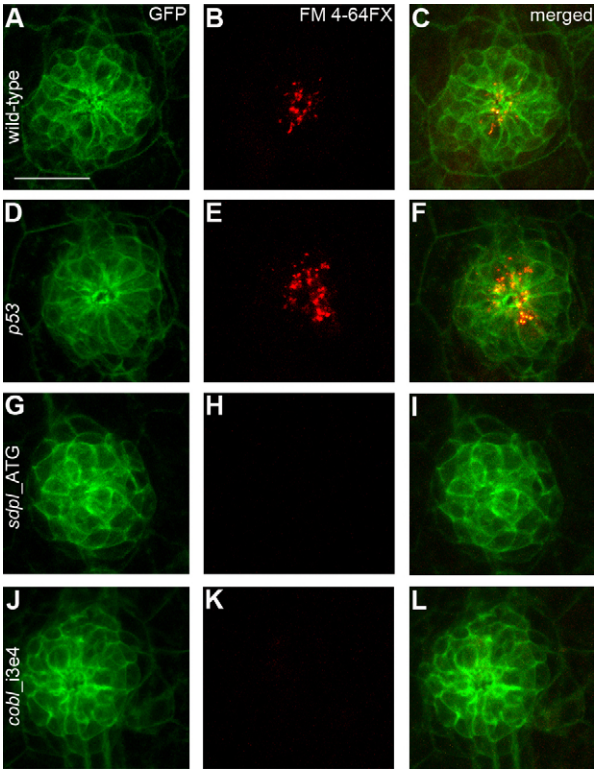

Fig. 5. Sensory hair cells within neuromasts of both *cobl*- and *syndapin I*-morphant zebrafish larvae are not functional. (**A**,**D**,**G**,**J**) Confocal images of representative posterior lateral line neuromasts of wild-type, *p53*-, *sdpl*- and *cobl*-morphant transgenic *claudinB:lyn(GFP)* larvae at 4 dpf. Hair cells are organized symmetrically in rosettes in wild-type (A), control-injected (D), *syndapin I* (G) and *cobl* morphants (J). (**B**,**E**,**H**,**K**) FM 4-64FX vital dye labeling shows a lack of dye uptake in *syndapin I* (H) and *cobl* (K) morphants in comparison with wild-type (B) and control-injected larvae (E). (**C**,**F**,**I**,**L**) Merged images of the mostly apical FM-labeling of vesicular structures and claudin-GFP. Scale bar: 20 µm.

localized to forming cilia. As for GFP- and mCherry-syndapin I (Fig. 7D–F,J–M), endogenous syndapin I of the ZF4 cells also localized to the basis of forming cilia (Fig. 7P–R). Together, these data suggest that syndapin I and Cobl are effectors during early cilia formation.

Co-injection of syndapin I mRNA rescues MO *sdpl*_e3i3-induced defects

For rescue experiments we next analyzed neuromasts formation in *claudinB:lyn(GFP)* embryos injected with a high dose of MO *sdpl*_e3i3 and in embryos injected with a combination of MO *sdpl*_e3i3 and mRNA encoding for syndapin I. The phenotype elicited by 0.4 pmol MO *sdpl*_e3i3 was more robust than with low doses (Fig. 4; 0.2 pmol) and thus suitable for rescue experiments. Although limited by instability of injected mRNA, MO *sdpl*_e3i3 defects at 48 hpf were indeed strongly suppressed by co-injection of full-length *syndapin I* mRNA (Fig. 8A,B).

Quantitative determinations showed that the number of neuromasts was restored from 2.8 to almost 4, whereas control larvae had ~5 neuromasts (Fig. 8E). Remarkably, this rescue of ~50% of the MO *sdpl*_e3i3 phenotype was obtained despite the fact that injection of *syndapin I* mRNA alone had some, albeit moderate, negative effects on neuromast formation (Fig. 8E). The successful suppression of the MO *sdpl*_e3i3 phenotype by *syndapin I* mRNA co-injection demonstrated the specificity of the syndapin I loss-of-function phenotypes observed upon MO *sdpl*_e3i3 injection.

The syndapin I F-BAR domain is required for rescuing MO *sdpl*_e3i3-induced defects

Considering the plasma membrane-binding ability shown for the F-BAR domains of mammalian syndapin isoforms (Dharmalingam et al., 2009), syndapin I may associate with membrane areas prone to cilia formation, recruit its SH3 domain binding partner Cobl and elicit local changes in membrane topology, which promote the formation of cilia (Fig. 8). If this would be the case, then cilia formation should rely on the lipid-binding and membrane curvature-sensing F-BAR domain of

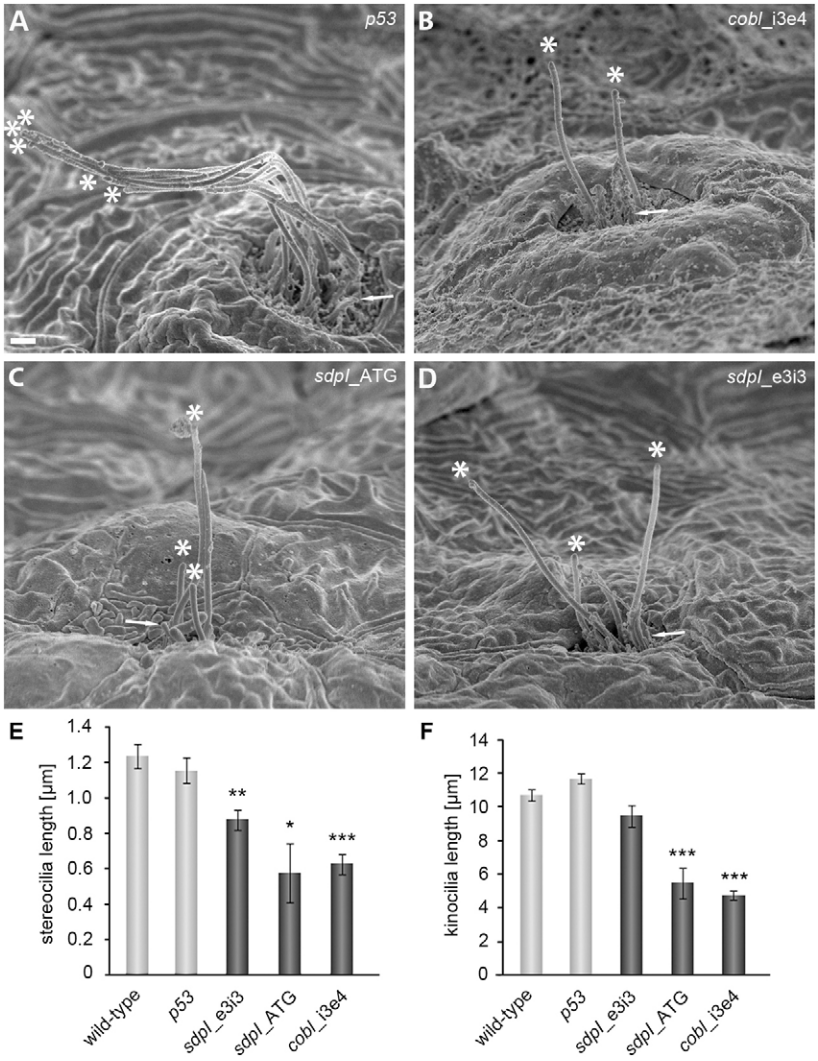

Fig. 6. Both F-actin-rich stereocilia and microtubule-based kinocilia are defective in *cobl* and *sdpl* morphants. (**A–D**) SEM images of hair cells of neuromasts of zebrafish embryos injected as indicated at 72 hpf. In both *cobl*- (B) and *sdpl*-morphant fish (C,D), kinocilia are reduced in number and significantly shortened. Tips of kinocilia are marked by asterisks. F-actin-rich stereocilia (arrows in A–D mark examples) also are severely affected. Scale bar: 1 µm. (**E**,**F**) Quantitative analyses of observable stereocilia (E) and kinocilia (F). Wild-type, $n=99$ kinocilia/82 stereocilia; control MO *p53*, $n=80$ kinocilia/17 stereocilia; MO *sdpl*_e3i3, $n=37$ kinocilia/38 stereocilia; MO *sdpl*_ATG, $n=10$ kinocilia/5 stereocilia; MO *cobl*_i3e4, $n=58$ kinocilia/19 stereocilia. Statistical analyses were performed versus wild-type. $^{*}P<0.05$, $^{**}P<0.01$, $^{***}P<0.001$. Kinocilia defects observed in *cobl* and *syndapin I* morphants (F) show even higher statistical significances versus MO *p53*-control (not depicted), MO *sdpl*_e3i3 (**), MO *sdpl*_ATG (***) and MO *cobl*_i3e4 (***).

syndapin I. Co-injection of mRNA encoding for a syndapin I mutant lacking the F-BAR domain (*sdpl*_SH3) together with MO *sdpl*_e3i3 indeed did not rescue the syndapin I loss-of-function phenotype but rather led to even stronger impairments in neuromast formation. Expression of the syndapin I SH3 domain was ensured and validated by fusion to mCherry (data not shown), which also did not rescue the MO *sdpl*_e3i3-mediated impairments, as shown in further control experiments (Fig. 8C–E).

Likewise, co-injection of mRNA encoding for a syndapin I mutant lacking the SH3 domain did not rescue MO *sdpl*_e3i3-induced impairments of neuromasts formation. Most embryos died but the few surviving showed fewer than three neuromasts on average and thus resembled MO *sdpl*_e3i3-injected embryos (not shown).

Thus, in line with a model, in which syndapin I serves as a spatial cue for Cobl recruitment (Fig. 8), neither membrane binding by the F-BAR domain nor Cobl binding by the syndapin I SH3 domain was sufficient but both molecular functions are critical for syndapin I function.

Co-injection of *cobl* mRNA suppresses Cobl loss-of-function phenotypes

Co-injection of mRNA encoding for full-length Cobl in combination with a high dose of MO *cobl*_i3e4 (0.4 pmol), which, in comparison to the lower-dose injections (Fig. 4H, 0.2 pmol), led to more severely shortened anterior–posterior body axes, curved body shapes, smaller heads and eyes, oedema in heart and brain (Fig. 8F,I) and also to a more dramatic reduction of neuromasts numbers (Fig. 8L,R), led to a dose-dependent suppression of the Cobl loss-of-function phenotypes (Fig. 8G,H,J,K,M). The bodies of larvae in these rescue experiments were straight and more elongated (Fig. 8F–H), ventricles were smaller and eyes larger (Fig. 8I–K) and neuromast numbers more than doubled in comparison to MO *cobl*_i3e4-injected embryos (Fig. 8L,M,R).

Cobl overexpression is very difficult to elicit in mammalian cells of different origin (Ahuja et al., 2007; Schwintzer et al., 2011; Haag et al., 2012). Likewise, expression of Cobl protein could not directly be visualized in 48 hpf larvae. We therefore verified that not a putative titrating-out of the MO but indeed Cobl protein expression was underlying the observed rescue effects. Co-injection of a mutant *cobl* mRNA (*cobl*^{mut}), which is still able to bind the MO but harbors a point mutation inserting a premature stop codon, failed to suppress the Cobl depletion phenotypes. Neither the eyes, not the body shape nor the number of neuromasts was improved in comparison to MO *cobl*_i3e4-injected embryos (Fig. 8L,N,R). Thus, suppression of the MO

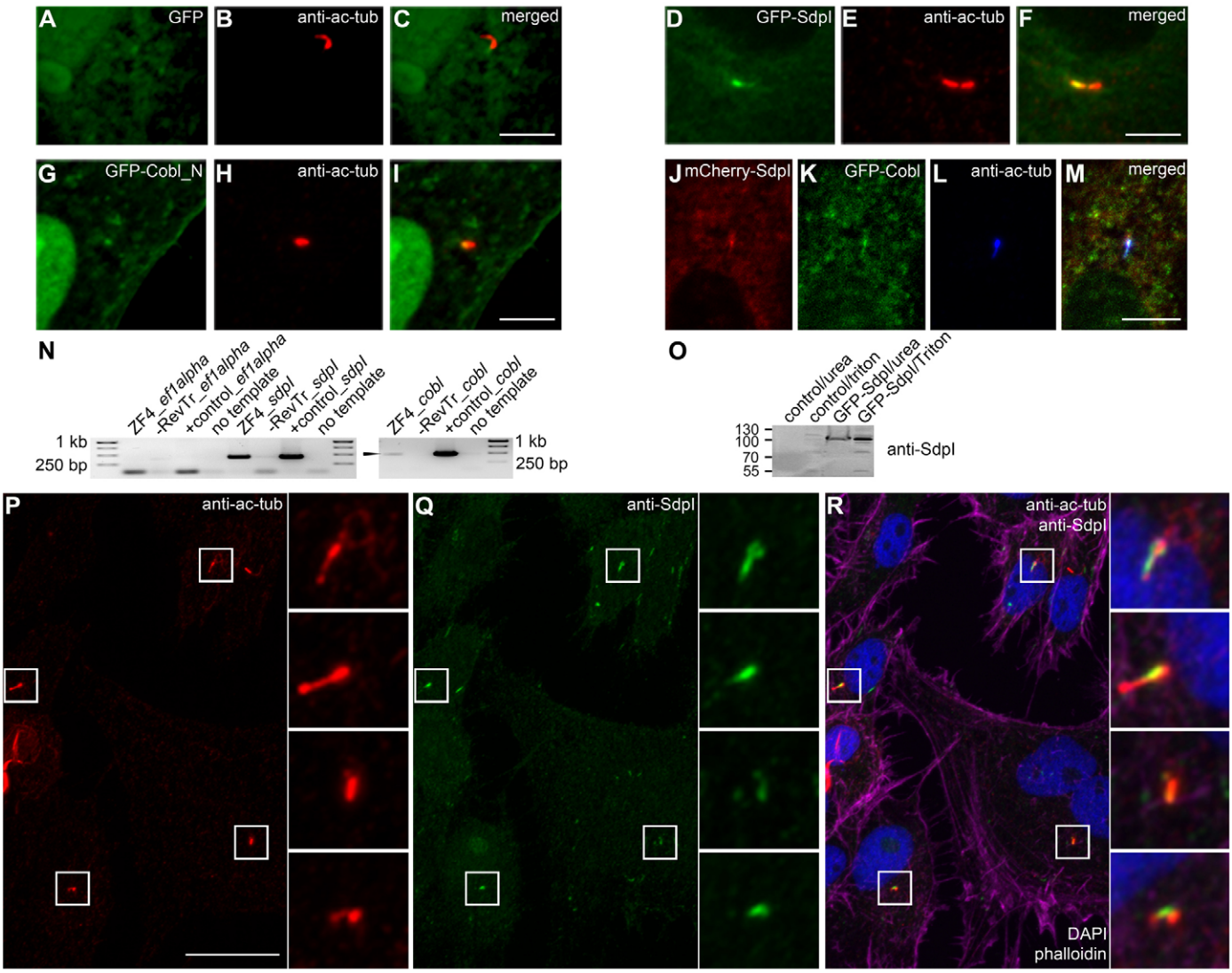

Fig. 7. Syndapin I and Cobl localize to the base of forming cilia. (**A–M**) Localization of GFP (A), GFP-syndapin I (D) and GFP-Cobl_N (G), as well as of a combination of mCherry-syndapin I (J) and GFP-Cobl (K) in ZF4 cells in relation to cilia marked by anti-acetylated-tubulin antibodies (B,E,H,L). In merged images, co-localizations appear yellow in (C,F,I) and white in (M). Scale bars: 5 µm. (**N**) RT-PCR analysis of ZF4 cell RNA for *syndapin I* and *cobl*. DNA plasmids were used as positive controls (+control) and *ef1alpha* served as a technical control. Both *syndapin I* and *cobl* (marked) were detected. (**O**) Affinity-purified anti-syndapin I antibodies specifically recognize zebrafish GFP-syndapin I overexpressed in HEK293 cells in immunoblotting analyses. (**P–R**) Acetylated tubulin (P) and endogenous syndapin I (Q) in ZF4 cells. The merged image (R) additionally includes phalloidin (purple) and DAPI (blue) labeling. Insets, magnifications of boxed areas. Scale bar: 20 µm.

*cobl*_i3e4-induced phenotype was specifically mediated by replenishing Cobl protein.

The actin-nucleating Cobl WH2 domains are not sufficient to rescue *cobl* MO-induced phenotypes, but Cobl's role in neuromast formation additionally requires the syndapin I-binding N-terminal part of Cobl

Since re-expression of full-length Cobl led to a highly significant suppression of the Cobl loss-of-function phenotypes, we next tested Cobl mutants that either lacked the syndapin I binding region but contained the actin-nucleating WH2 domains (Cobl_C) or lacked the C-terminal region important for actin nucleation but contained the syndapin I-binding N-terminal part (Cobl_N). Interestingly, both of these two Cobl mutants, whose expression was verified by mCherry-tagging, as well as the corresponding mCherry control, failed to rescue the Cobl loss-of-function phenotypes in both proper development of the body and neuromast formation (Fig. 8O–R).

These results demonstrate that Cobl's critical role in formation of functional lateral line organs requires both known functional domains of Cobl, the syndapin I-binding N-terminal part and the actin-nucleating C-terminal part. Thus, proper formation of sensory hair cells seems to rely on formation of syndapin I complexes with the actin nucleator Cobl and additionally on membrane topology-modulating mechanisms involving syndapin I's F-BAR domain functions.

Discussion

Development and maintenance of defined cell shapes is a complex task. Ciliogenesis is a prime example for a spatially

well-defined modulation of plasma membrane topology. Primary cilia of hair cells of the inner ear and of neuromasts of the lateral line organ of fish are crucial for sensory functions. We here show at the whole animal level that reduced levels of the actin nucleator Cobl as well as of the F-BAR protein syndapin I cause severe defects in proper sensory organ formation and function. These defects are in line with the restricted expression patterns of both genes. Zebrafish *syndapin I* displayed an exclusive expression in neuromasts of the posterior and anterior lateral line as well as in the nervous system. Consistently, mammalian syndapin I is mainly expressed in brain and retina (Qualmann et al., 1999; Koch et al., 2011). Expression in the inner ear can also be detected (our unpublished observations). *Cobl* expression in zebrafish was found in the same tissues. Additionally, some

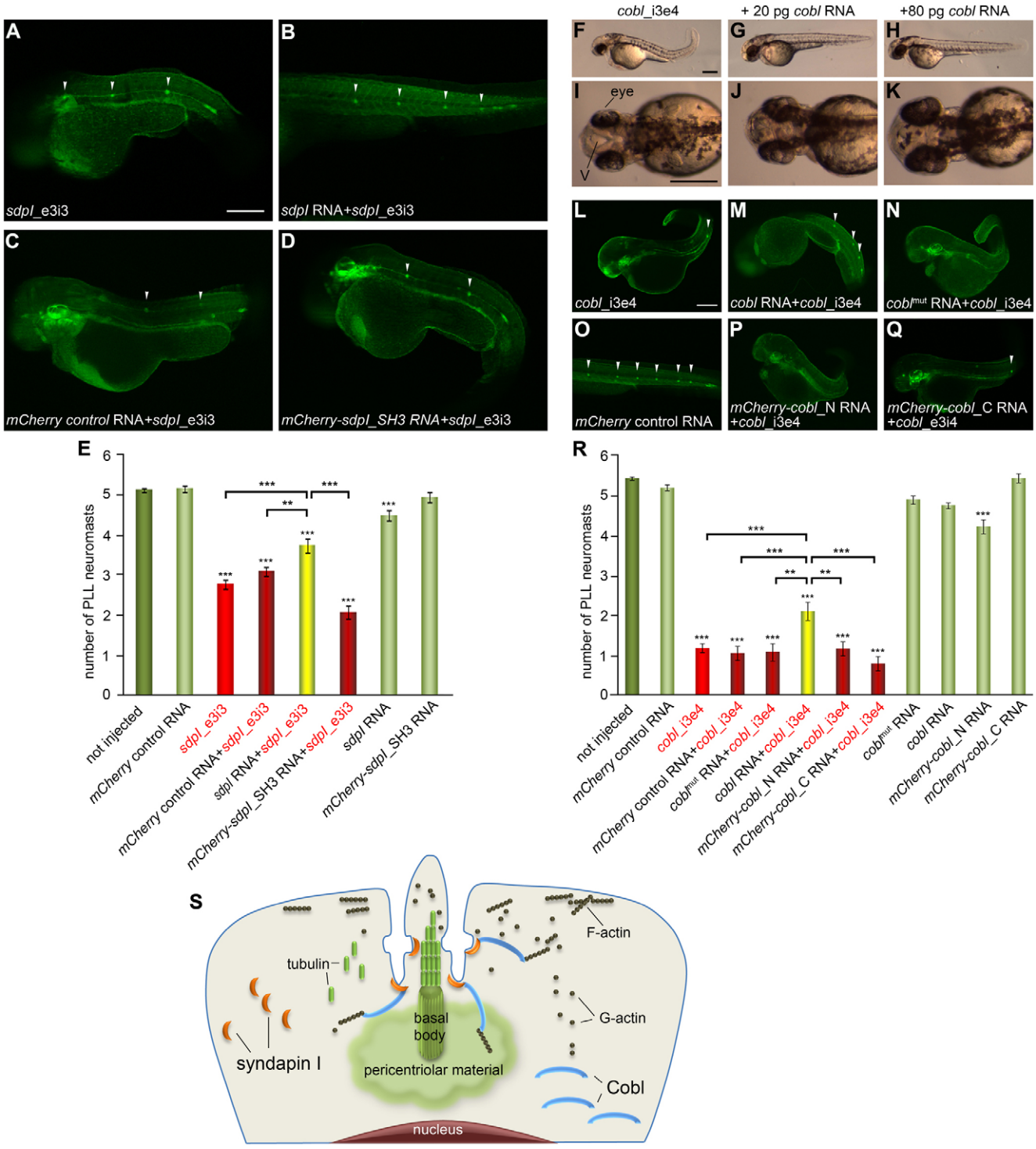

Fig. 8. See next page for legend.

cobl expression was found in somites and the pronephric duct. The latter is consistent with previous observations of some Cobl function in motile cilia of Kupffer's vesicle and thus for left/right determination (Ravanelli and Klingensmith, 2011). The expression of both *cobl* and *syndapin I* in neuromasts during their maturation and the strong cilia defects observed in *cobl*- and *syndapin I*-morphant fish clearly show that, besides playing some role in motile cilia, both proteins are essential for the formation of non-motile cilia and for sensory hair cell function.

Ciliopathies are connected with several human diseases (Gerdes et al., 2009; Lee and Gleeson, 2011; Goetz and Anderson, 2010). Ciliopathies include early developmental defects like failures in left/right patterning. Furthermore, a curved and shortened body axis is the most prominent defect observed in zebrafish embryos with ciliary defects (Malicki et al., 2011). All of these developmental defects were observed both in *cobl* and *syndapin I*-morphant animals. Cilia also play a pivotal role in inner ear functions in mammals. The respective organ in fish is the lateral line. They are essential for balance keeping and orientation in space. Consistent with their sensory hair cell defects, both *cobl* and *syndapin I* morphants displayed severe defects in balance keeping and aberrant and uncoordinated swimming behaviors.

Mechanosensory hair cells of the lateral line each contain a single microtubule-rich kinocilium and several F-actin-rich stereocilia (Ma and Raible, 2009). Mechanistically, the early events that shape the apical compartment and give rise to the different ciliary structures are not well understood. A dramatic loss and truncation of stereocilia and kinocilia similar to that observed in *cobl* and *syndapin I* morphants had previously been observed upon neomycin or heavy metal exposure (Harris et al., 2003) and in *tmie*- and *rab escort protein 1*-deficient zebrafish. Interestingly, *tmie* and *rab escort protein 1*-deficient zebrafish to a large extent also showed spinning movements (Gleason et al., 2009; Starr et al., 2004). Functional genomic screens identified protein transport as well as actin cytoskeletal components as ciliogenesis modulators (Kim et al., 2010). In line with this, Cobl is an actin nucleator (Ahuja et al., 2007; Husson et al., 2011) and syndapin I plays a role in dynamin-mediated vesicle formation processes originating from the plasma membrane (Andersson et al., 2008; Anggono et al., 2006; Koch et al., 2011; Koch et al., 2012; Qualmann and Kelly, 2000). Moreover, syndapin I controls rearrangements of the cortical cytoskeleton by combining its lipid-binding ability with SH3 domain interactions, such as those with the Arp2/3 complex activator N-WASP and with the actin nucleator Cobl (Qualmann and Kelly, 2000; Kessels and Qualmann, 2002; Kessels and Qualmann, 2006; Dharmalingam et al., 2009; Schwintzer et al., 2011).

Syndapin I and *cobl* morphants both showed a dramatic loss of stereocilia and kinocilia emanating from the apical surface of hair cells. Both structures are formed after neuromast deposition, i.e. after ~48 hpf. In line with this, expression of *cobl* and *syndapin I* within the posterior lateral line became readily detectable in 72 hpf embryos, while it remained low during the time of primordium migration.

Stereocilia are marked by polarized, dynamic bundles of unbranched actin filaments (Manor and Kachar, 2008). It is therefore well conceivable that proteins promoting actin filament formation, such as Cobl, play important roles in the establishment, elongation and/or maintenance of stereocilia. Indeed, β-actin-deficient murine hair cells showed stereocilia defects (Perrin et al., 2010) that are similar to those of *syndapin I* and *cobl* morphants. Furthermore, one formin family member, mDia1, is implicated in non-syndromic progressive deafness (Lynch et al., 1997) and therefore was suggested to play some role in stereocilia maintenance (Zigmond, 2004). Vangl2, which shows some genetic interaction with *cobl* in neural tube formation in mice (Carroll et al., 2003), was recently observed to be important for tilting motile cilia at the floorplate of zebrafish by unknown mechanisms (Borovina et al., 2010). Cobl, which is important for apical F-actin in Kupffers vesicles, had been observed apically when fused to GFP, and this localization was dependent on its N-terminal parts and not on the actin nucleating C-terminus (Ravanelli and Klingensmith, 2011). As an explanation for this observation, we show that the N-terminal part of zebrafish Cobl binds syndapin I. Consistently, KrrAPpPP motifs conserved within the N-terminal domain of mammalian and teleost Cobl were revealed as binding sites for syndapins in mammals (Schwintzer et al., 2011). Syndapin II was dynamically enriched at the apical membrane of acinar cells of the lacrimal gland (da Costa et al., 2003). Syndapins bind to phosphatidyl-inositol-(4,5)-bisphosphate and phosphatidylserine targeting them specifically to the plasma membrane (Itoh et al., 2005; Dharmalingam et al., 2009) and syndapin I can promote membrane recruitment of Cobl in rat hippocampal neurons (Schwintzer et al., 2011). Together, these data suggest that Cobl/syndapin I complexes shape certain membrane areas.

The exact role of the actin cytoskeleton in cilia formation, elongation and/or maintenance is unknown. Local actin dynamics may be required to promote microtubule-driven ciliogenesis and cilia growth (Bershteyn et al., 2010; Kim et al., 2010). Recent work (Werner et al., 2011) showed that some intricate interplay between actin and microtubules is required to coordinate cell

Fig. 8. Syndapin I and Cobl protein domain functions reflecting syndapin I/Cobl complex formation, Cobl-mediated actin nucleation and syndapin I-mediated plasma membrane association are crucial for restoring proper formation of neuromasts. (**A–D**) Co-injection of MO *sdpI*_e3i3 (0.4 pmol) with *syndapin I* mRNA (B) but not with mRNA encoding mCherry (control; C) or the mCherry-syndapin I SH3 domain (D) into *claudinB:lyn(GFP)* embryos rescued MO *sdpI*_e3i3-induced defects. (**E**) Quantification of neuromast numbers (not injected, $n=173$; *mCherry* control RNA, $n=103$; *sdpI*_e3i3 $n=86$; *mCherry* control RNA+*sdpI*_e3i3, $n=66$; *sdpI* RNA+*sdpI*_e3i3, $n=57$; *mCherry sdpI*_SH3 RNA+*sdpI*_e3i3, $n=60$. *sdpI* RNA, $n=56$; *mCherry sdpI*_SH3 RNA, $n=40$. (**F–K**) Dose-dependent rescue of Cobl loss-of-function phenotypes (0.4 pmol MO *cobl*_i3e4) at 48 hpf by re-expression of Cobl (by injection of 20 pg (G,J) and 80 pg (H,K) *cobl* mRNA, respectively) in *claudinB:lyn(GFP)* embryos. Note the increasingly straight and elongated body axes (lateral body views, F–H) and the suppressed defects of the brain (v, ventricle) and eyes in *cobl* mRNA-co-injected embryos (dorsal head views, I–K). (**L–Q**) Injection of mRNA encoding full-length Cobl but none of the other indicated RNA injections rescued the MO *cobl*_i3e4-mediated impairments of proper body and neuromast development. Arrowheads mark *claudinB:lyn(GFP)* neuromasts. Scale bars: 250 µm. (**R**) Quantification of neuromasts of *claudinB:lyn(GFP)* zebrafish injected as indicated. Not injected, $n=190$; *mCherry* control RNA, $n=82$; *cobl*_i3e4, $n=124$; *mCherry* control RNA+*cobl*_i3e4, $n=43$; $cobl^{mut}$ RNA+*cobl*_i3e4, $n=27$; *cobl* RNA+*cobl*_i3e4, $n=45$; *mCherry-cobl*_N RNA+*cobl*_i3e4, $n=33$; *mCherry-cobl*_C RNA+*cobl*_i3e4, $n=50$, $cobl^{mut}$ RNA, $n=36$; *cobl* RNA, $n=59$; *mCherry-cobl*_N RNA, $n=38$; *mCherry-cobl*_C RNA, $n=33$. Statistical analyses, ANOVA with Tukey's test versus mCherry control-injection (marked above each column). Significant differences of non-rescues versus rescues are also marked. $^{**}P<0.01$, $^{***}P<0.001$. (**S**) Model depicting syndapin I and Cobl in early cilium formation.

polarity of multiciliated cells. Observations in MDCK cells suggested that one function of actin structures may be to provide a diffusion barrier between the ciliary and plasma membrane (Francis et al., 2011), which manifests in different lipid and protein composition (Nachury et al., 2010).

The similar phenotypes we observed in *cobl* and *syndapin I* loss-of-function analyses irrespective of whether kinocilia, motile cilia and stereocilia-dependent functions were analyzed suggest a common mechanistical feature. Since syndapins were suggested to be curvature-sensing and/or inducing F-BAR proteins (Qualmann et al., 2011), the unifying feature in kinocilia, motile cilia and stereocilia formation may be the need to locally generate a sharp positive membrane curvature at the base of all of these structures. In line with this, syndapin I was localized to the base of cilia early during ciliogenesis. Furthermore, our rescue experiments demonstrated that syndapin I's role in neuromast formation required functions of the syndapin I F-BAR domain. The hypothesis that BAR domains are important modules for shaping membranes (Peter et al., 2004) also is underscored experimentally by the recent finding that syndapin I deficiency led to aberrant curvatures of synaptic vesicles in mouse neurons (Koch et al., 2011).

High membrane curvature at the cilia base was suggested to contribute to the diffusion restriction (Breslow and Nachury, 2011). Curved membrane areas are especially elaborate in cilia with prominent ciliary pockets. Interestingly, these structures have recently been proposed to represent actin/cilium interfaces (Ghossoub et al., 2011; Molla-Herman et al., 2010). Syndapin I is able to oligomerize (Kessels and Qualmann, 2006) and to form protein lattices at lipid surfaces (Frost et al., 2008). It is conceivable that such membrane-associated scaffolds contribute to restricting lateral diffusion in the membrane. Furthermore, both syndapin I self-association and lipid binding does not involve syndapin I's SH3 domain (Kessels and Qualmann, 2006; Dharmalingam et al., 2009) and thereby leaves this domain available for complex formation with actin-modulating molecules, such as the actin nucleator Cobl. Consistently, syndapin I's interaction with Cobl was SH3 domain-mediated and the syndapin SH3 domain was crucial for rescuing syndapin I depletion phenotypes in neuromast formation. Vice versa, mutants lacking the syndapin I-binding part of Cobl were unable to rescue Cobl loss-of-function phenotypes.

Together, our loss-of-function studies not only reveal the individual functions of syndapin I and its binding partner Cobl in different ciliogenesis processes at the whole animal level but furthermore strongly suggest that the impairments we observed explicitly reflect functions of Cobl/syndapin I protein complexes localized to plasma membrane areas at the base of forming cilia by the ability of the syndapin I's F-BAR domain to associate with positively curved plasma membrane structures (for model see Fig. 8). This conclusion is based on the fact that the expression patterns of zebrafish *cobl* and *syndapin I* overlap, that the two proteins interact physically, that *cobl* and *syndapin I* knock-down lead to very similar phenotypes and that these depletion phenotypes are rescued upon re-expression of wild-type Cobl and syndapin I proteins but not upon re-expression of mutants defective in Cobl/syndapin I complex formation.

Taken together, the defects in proper body laterality and axis establishment and in ciliogenesis of hair cells of the posterior lateral line as well as the behavioral phenotypes, which relate to these defects, such as uncoordinated swimming as well as severe impairments in balance keeping, all strongly suggest that the actin nucleator Cobl and the F-BAR protein syndapin I work together intimately in ciliogenesis.

Materials and Methods

Zebrafish maintenance

Zebrafish (strain AB Tübingen) were maintained under standard conditions (Westerfield, 1992) and in compliance with the German Animal Welfare Law. The transgenic strain *claudinB:lyn(GFP)* was kindly provided by D. Gilmour. Embryos were collected and raised in egg water at 28.5°C. Staging was performed according to Kimmel et al. (Kimmel et al., 1995).

RNA preparation and cDNA synthesis

Total mRNA was prepared from ~20 embryos or larvae for each stage. Animals were lyzed with 350 µl buffer RLT (including 0.1 mM DDT) according to protocol (RNeasy kit; Qiagen).

DNA was digested with DNase (on column; Qiagen) prior to reverse transcription. RNA from ZF4 cells was prepared with TRIZOL reagent (Invitrogen) according to manufacturer's instruction (yield, ~50 µg RNA/25 cm^2 flask).

Reverse transcription was done with 0.5 µg RNA (corresponding to RNA from around 2 embryos) using Superscript II (Invitrogen) and oligo-dT primer in a volume of 20 µl (42°C, 1 h 15 min).

RNA synthesis and RNA injection

Capped mRNA encoding for syndapin I, Cobl and mutants thereof, respectively, was prepared by cloning of the respective sequences into pCS2+ vector, linearization and *in vitro* transcription with the mMessagemMachine SP6 Kit (Ambion, Life technologies) according to manufacturer's instruction. The RNA was purified and injected into in the yolk of 1- to 2-cell embryos as described (20–80 pg).

DNA constructs and protein preparation

Plasmids encoding syndapin I, syndapin I SH3 domain (SdpI_SH3; aa381–445), Cobl full-length (aa1–1312), as well as the Cobl N- (Cobl_N; aa1–295) and the Cobl C-terminus (Cobl_C; aa1060–1312) were generated by PCR using cDNA of 24 hpf or 7 dpf embryos (primer sequences: sdpI, CG**GAATTC**atgtcgggtgcctacgatg, CGC**GTCGAc**taaacaggttccacatagtttg; fwd SH3, CG**GAATTC**ATGccatttgaagag-gacagtaa; cobl, CG**GAATTC**atgaaggcccaggctccccctcc, C**GCTCGAG**ttagtgtccgta-agagaggggtgatg; rev N-term, C**GCTCGAG**tcatgctggagctctgcgtttct, fwd C-term, ATGgtgtctgctcacattaaatcctt). PCR products were cloned into pGEM-Teasy (Promega) and into pGEX-5×1 (GE Healthcare), respectively, and sequenced. GFP-derivatives were obtained by subcloning into pEGFP-C2 (BD Biosciences).

A Cobl mutant with a premature stop inserted at position 4 used as template for mutated Cobl mRNA generation was generated by primer mutagenesis and cloned into pCS2+.

GST and GST-SdpI_SH3 were prepared as described (Qualmann and Kelly, 2000).

Antibodies and reagents

Anti-zebrafish syndapin I antibodies were obtained by affinity-purifying rabbit antibodies directed against mammalian syndapin I (Qualmann et al., 1999) with HisTrx-tagged zebrafish syndapin I according to Qualmann et al. (Qualmann et al., 1999). The purified antibodies were characterized by immunoblotting with GFP-zebrafish syndapin I expressed in HEK293 cells. HisTrx-syndapin I was purified according to Schwintzer et al. (Schwintzer et al., 2011).

Commercially available antibodies and fluorescent reagents used include: mouse anti-acetylated-tubulin 6-11b-1 (Sigma), rabbit anti-GFP (Abcam), AlexaFluor488 goat anti-mouse and anti-rabbit, AlexaFluor568 goat anti-mouse, and AlexaFluor488-, and AlexaFluor647- and AlexaFluor568-conjugated phalloidin and FM 4-64FX (Invitrogen).

Co-precipitation experiments

Co-precipitation experiments with GST and GFP-fusion proteins expressed in HEK293 cells were performed as described (Qualmann and Kelly, 2000; Kessels and Qualmann, 2006) and analyzed by anti-GFP immunoblotting.

HEK293 cell lysates for characterization of anti-zebrafish syndapin I antibodies by western blotting were prepared by lysis in 8 M Urea or by Triton X-100 extraction (Qualmann and Kelly, 2000; Kessels and Qualmann, 2006).

Antisense MO injections

MOs were obtained from GeneTools and injected in the yolk of 1- to 2-cell embryos as described (1 mM) (Perner et al., 2007). Injection volumes were calculated according to Perner et al. (Perner et al., 2007). Robust phenotypes for *syndapin I* and *cobl* morphants were obtained with 0.4 nl (0.4 pmol), 0.2 nl (0.2 pmol) and 0.1 nl (0.1 pmol) MO, respectively. For MO *cobl*_e4i4, the highest

injection volume applied was 1.2 pmol. The sequences of MOs were, *sdpl*_ATG, CGTAGGCACCCGACATGCTGAGAGA; *sdpl*_e3i3, GTTGTCTCACTGACC-CTTCTCGATG; *cobl*_i3e4, ATCCATCAGAGCTTTTCTGAAGAGA; *cobl*_e4i4, GTTACAGACACTCACCTCTGGCACT; *p53* GCGCCATTGCTTTGCAAGAA-TTG (GeneTools).

In situ hybridizations

Syndapin I full-length and *cobl*_N in pGEM-Teasy served as templates for RNA probe generation. *Eya1*- and *pitx2*-specific probes were described (Campione et al., 1999; Landgraf et al., 2010). After linearization, digoxygenin-labeled sense (controls) and antisense riboprobes were synthesized according to manufacturer's protocol (Roche). Whole mount *in situ* hybridizations were performed as described (Perner et al., 2007). Images were captured using a Zeiss DiscoveryV8 microscope with Achromat-S objectives (2.0× to 8.0×) and a ProgRes-C10plus camera (Jenoptik) and were analyzed with Axiovision (Zeiss) and ImageJ. Images were processed using Adobe Photoshop.

ZF4 cell maintenance and primary cilia induction

ZF4 cells (Driever and Rangini, 1993) were maintained in DMEM F12 (Invitrogen) with 10% FCS at 29℃. Transfections were done with X-tremeGene HP (Roche) according to the instruction of the manufacturer. Primary cilia were induced by serum-starvation. Cells were fixed with 4% PFA after 5 and 24 h of serum starvation, respectively, and processed for immunofluorescence analyses according to Kessels et al. (Kessels et al., 2000).

Antibodies, whole mount immunohistochemistry and fluorescence microscopy of zebrafish

Embryos or larvae were fixed overnight in 4% PFA in 0.1% Tween-containing PBS (PBS-T) at 4℃. After permeabilization with 1% Triton X-100 in PBS-T at RT (24 hpf, 1 h; 48 hpf, 2 h; 72 hpf, 4 h; 5 dpf, 6 h), several washes in PBS-T and blocking in 10% horse serum, 1% BSA, 1% DMSO in PBS-T for 1 h at RT, embryos were incubated overnight with primary antibody at 4℃. Secondary antibody incubations were done for 1.5 h at RT. After several washing steps with PBS-T (5×5 min, 5×20 min) at RT, embryos were embedded in low melting agarose.

Images were taken with an Axio Observer.Z1 (Zeiss) using 20× dry objectives and 40× and 63× oil immersion objectives, respectively. Image acquisition and processing was performed using Axiovision4.8.2. Confocal images were recorded with a Leica TCS-SP5 with 20× and 40× dry objectives and a 63× oil immersion objective in z-sections of 0.5 µm (40×, 63×) and 1.0 µm (20×) slices, respectively.

Posterior lateral line neuromasts were counted based on *eya1 in situ* and *claudinB:lyn(GFP)* signals. The terminal cluster of neuromasts was not included. Body axis lengths at 24 hpf stages were measured by analyzing the trunk length from the first to the last somite with ImageJ.

SEM analysis

72 hpf embryos were collected and fixed overnight in 4% glutaraldehyde at 4℃. After 2×5 min washing with sterile water and tube changing, three further washes followed. The embryos were dehydrated (10%, 20%, 30%, 50%, 70%, 80%, 90%, 100% ethanol; 20 min each) and critical point-dried in liquid CO_2. Embryos were sputtered with gold and analyzed with a LEO1530 Gemini FESEM (Zeiss). SEM images of neuromasts were recorded at angles of about 30° from the body surface and kinocilia and stereocilia were measured, if resolved completely.

Behavior analysis

Embryos at 48 hpf were dechorionated and stimulated via tail taps with ultrafine tips immediately thereafter. Several experiments were conducted and quantified for each condition.

Video clips were captured with a CanonEOS 500D camera (Canon). Tracking of swim paths was done with ImageJ.

Vital dye labeling

Transgenic *claudinB:lyn(GFP)* larvae were placed in 50 ml tubes equipped with a mesh at the bottom allowing free swimming but also very fast medium exchange. Hair cells were stained by incubation with 3 µM FM 4-64FX (Invitrogen, Carlsbad, CA) in embryo medium (Kimmel et al., 1995) for 30 s at RT. After three rinses in embryo medium, larvae were fixed in 4% PFA, embedded in low melting agarose and analyzed via confocal microscopy as described above.

Statistical analysis

Results were calculated as means±s.e.m. Statistical analysis was performed using one-way ANOVA and Tukey's multiple comparison test.

Acknowledgements

We thank E. Rivera-Milla and F. Bollig for MO design and C. Ebert, C. Hahn and A. Kreusch for technical assistance, M. Westermann and S. Linde (EM-Centre, Jena University Hospital), for help with SEM, A. Dorn for video clip acquisition and L. McMillan for manuscript proofreading. We furthermore thank M. Blum and A. Schweikert for the *pitx2* probe and D. Gilmour for the *claudinB:lyn(GFP)* line.

Funding

This work was supported by the Deutsche Forschungsgemeinschaft (DFG) [grant numbers SFB604, project C7, to C.E., KE685/3-1 to M.M.K., Qu116/5-1 and 6-1 to B.Q. and Qu116/7-1 to M.M.K. and B.Q.].

Supplementary material available online at
http://jcs.biologists.org/lookup/suppl/doi:10.1242/jcs.111674/-/DC1

References

Ahuja, R., Pinyol, R., Reichenbach, N., Custer, L., Klingensmith, J., Kessels, M. M. and Qualmann, B. (2007). Cordon-bleu is an actin nucleation factor and controls neuronal morphology. *Cell* **131**, 337-350.

Andersson, F., Jakobsson, J., Löw, P., Shupliakov, O. and Brodin, L. (2008). Perturbation of syndapin/PACSIN impairs synaptic vesicle recycling evoked by intense stimulation. *J. Neurosci.* **28**, 3925-3933.

Anggono, V., Smillie, K. J., Graham, M. E., Valova, V. A., Cousin, M. A. and Robinson, P. J. (2006). Syndapin I is the phosphorylation-regulated dynamin I partner in synaptic vesicle endocytosis. *Nat. Neurosci.* **9**, 752-760.

Bershteyn, M., Atwood, S. X., Woo, W. M., Li, M. and Oro, A. E. (2010). MIM and cortactin antagonism regulates ciliogenesis and hedgehog signaling. *Dev. Cell* **19**, 270-283.

Borovina, A., Superina, S., Voskas, D. and Ciruna, B. (2010). Vangl2 directs the posterior tilting and asymmetric localization of motile primary cilia. *Nat. Cell Biol.* **12**, 407-412.

Breslow, D. K. and Nachury, M. V. (2011). Primary cilia: how to keep the riff-raff in the plasma membrane. *Curr. Biol.* **21**, R434-R436.

Campione, M., Steinbeisser, H., Schweickert, A., Deissler, K., van Bebber, F., Lowe, L. A., Nowotschin, S., Viebahn, C., Haffter, P., Kuehn, M. R. et al. (1999). The homeobox gene Pitx2: mediator of asymmetric left-right signaling in vertebrate heart and gut looping. *Development* **126**, 1225-1234.

Carroll, E. A., Gerrelli, D., Gasca, S., Berg, E., Beier, D. R., Copp, A. J. and Klingensmith, J. (2003). Cordon-bleu is a conserved gene involved in neural tube formation. *Dev. Biol.* **262**, 16-31.

da Costa, S. R., Sou, E., Xie, J., Yarber, F. A., Okamoto, C. T., Pidgeon, M., Kessels, M. M., Mircheff, A. K., Schechter, J. E., Qualmann, B. et al. (2003). Impairing actin filament or syndapin functions promotes accumulation of clathrin-coated vesicles at the apical plasma membrane of acinar epithelial cells. *Mol. Biol. Cell* **14**, 4397-4413.

Dharmalingam, E., Haeckel, A., Pinyol, R., Schwintzer, L., Koch, D., Kessels, M. M. and Qualmann, B. (2009). F-BAR proteins of the syndapin family shape the plasma membrane and are crucial for neuromorphogenesis. *J. Neurosci.* **29**, 13315-13327.

Driever, W. and Rangini, Z. (1993). Characterization of a cell line derived from zebrafish (Brachydanio rerio) embryos. *In Vitro Cell. Dev. Biol. Anim.* **29**, 749-754.

Edeling, M. A., Sanker, S., Shima, T., Umasankar, P. K., Höning, S., Kim, H. Y., Davidson, L. A., Watkins, S. C., Tsang, M., Owen, D. J. et al. (2009). Structural requirements for PACSIN/Syndapin operation during zebrafish embryonic notochord development. *PLoS ONE* **4**, e8150.

Francis, S. S., Sfakianos, J., Lo, B. and Mellman, I. (2011). A hierarchy of signals regulates entry of membrane proteins into the ciliary membrane domain in epithelial cells. *J. Cell Biol.* **193**, 219-233.

Frost, A., Perera, R., Roux, A., Spasov, K., Destaing, O., Egelman, E. H., De Camilli, P. and Unger, V. M. (2008). Structural basis of membrane invagination by F-BAR domains. *Cell* **132**, 807-817.

Gasca, S., Hill, D. P., Klingensmith, J. and Rossant, J. (1995). Characterization of a gene trap insertion into a novel gene, cordon-bleu, expressed in axial structures of the gastrulating mouse embryo. *Dev. Genet.* **17**, 141-154.

Gerdes, J. M., Davis, E. E. and Katsanis, N. (2009). The vertebrate primary cilium in development, homeostasis, and disease. *Cell* **137**, 32-45.

Ghossoub, R., Molla-Herman, A., Bastin, P. and Benmerah, A. (2011). The ciliary pocket: a once-forgotten membrane domain at the base of cilia. *Biol. Cell* **103**, 131-144.

Gleason, M. R., Nagiel, A., Jamet, S., Vologodskaia, M., López-Schier, H. and Hudspeth, A. J. (2009). The transmembrane inner ear (Tmie) protein is essential for normal hearing and balance in the zebrafish. *Proc. Natl. Acad. Sci. USA* **106**, 21347-21352.

Goetz, S. C. and Anderson, K. V. (2010). The primary cilium: a signalling centre during vertebrate development. *Nat. Rev. Genet.* **11**, 331-344.

Haag, N., Schwintzer, L., Ahuja, R., Koch, N., Grimm, J., Heuer, H., Qualmann, B. and Kessels, M. M. (2012). The actin nucleator cobl is crucial for Purkinje cell development and works in close conjunction with the F-actin-binding protein Abp1. *J. Neurosci.* **32**, 17842-17856.

Haas, P. and Gilmour, D. (2006). Chemokine signaling mediates self-organizing tissue migration in the zebrafish lateral line. *Dev. Cell* **10**, 673-680.
Harris, J. A., Cheng, A. G., Cunningham, L. L., MacDonald, G., Raible, D. W. and Rubel, E. W. (2003). Neomycin-induced hair cell death and rapid regeneration in the lateral line of zebrafish (Danio rerio). *J. Assoc. Res. Otolaryngol.* **4**, 219-234.
Hoegg, S., Brinkmann, H., Taylor, J. S. and Meyer, A. (2004). Phylogenetic timing of the fish-specific genome duplication correlates with the diversification of teleost fish. *J. Mol. Evol.* **59**, 190-203.
Husson, C., Renault, L., Didry, D., Pantaloni, D. and Carlier, M. F. (2011). Cordon-Bleu uses WH2 domains as multifunctional dynamizers of actin filament assembly. *Mol. Cell* **43**, 464-477.
Itoh, T., Erdmann, K. S., Roux, A., Habermann, B., Werner, H. and De Camilli, P. (2005). Dynamin and the actin cytoskeleton cooperatively regulate plasma membrane invagination by BAR and F-BAR proteins. *Dev. Cell* **9**, 791-804.
Kessels, M. M. and Qualmann, B. (2002). Syndapins integrate N-WASP in receptor-mediated endocytosis. *EMBO J.* **21**, 6083-6094.
Kessels, M. M. and Qualmann, B. (2004). The syndapin protein family: linking membrane trafficking with the cytoskeleton. *J. Cell Sci.* **117**, 3077-3086.
Kessels, M. M. and Qualmann, B. (2006). Syndapin oligomers interconnect the machineries for endocytic vesicle formation and actin polymerization. *J. Biol. Chem.* **281**, 13285-13299.
Kessels, M. M., Engqvist-Goldstein, A. E. and Drubin, D. G. (2000). Association of mouse actin-binding protein 1 (mAbp1/SH3P7), an Src kinase target, with dynamic regions of the cortical actin cytoskeleton in response to Rac1 activation. *Mol. Biol. Cell* **11**, 393-412.
Kim, J., Lee, J. E., Heynen-Genel, S., Suyama, E., Ono, K., Lee, K., Ideker, T., Aza-Blanc, P. and Gleeson, J. G. (2010). Functional genomic screen for modulators of ciliogenesis and cilium length. *Nature* **464**, 1048-1051.
Kimmel, C. B., Ballard, W. W., Kimmel, S. R., Ullmann, B. and Schilling, T. F. (1995). Stages of embryonic development of the zebrafish. *Dev. Dyn.* **203**, 253-310.
Koch, D., Spiwoks-Becker, I., Sabanov, V., Sinning, A., Dugladze, T., Stellmacher, A., Ahuja, R., Grimm, J., Schüler, S., Müller, A. et al. (2011). Proper synaptic vesicle formation and neuronal network activity critically rely on syndapin I. *EMBO J.* **30**, 4955-4969.
Koch, D., Westermann, M., Kessels, M. M. and Qualmann, B. (2012). Ultrastructural freeze-fracture immunolabeling identifies plasma membrane-localized syndapin II as a crucial factor in shaping caveolae. *Histochem. Cell Biol.* **138**, 215-230.
Landgraf, K., Bollig, F., Trowe, M. O., Besenbeck, B., Ebert, C., Kruspe, D., Kispert, A., Hänel, F. and Englert, C. (2010). Sipl1 and Rbck1 are novel Eya1-binding proteins with a role in craniofacial development. *Mol. Cell. Biol.* **30**, 5764-5775.
Lee, J. E. and Gleeson, J. G. (2011). Cilia in the nervous system: linking cilia function and neurodevelopmental disorders. *Curr. Opin. Neurol.* **24**, 98-105.
Lopes, S. S., Lourenço, R., Pacheco, L., Moreno, N., Kreiling, J. and Saúde, L. (2010). Notch signalling regulates left-right asymmetry through ciliary length control. *Development* **137**, 3625-3632.
Lynch, E. D., Lee, M. K., Morrow, J. E., Welcsh, P. L., León, P. E. and King, M. C. (1997). Nonsyndromic deafness DFNA1 associated with mutation of a human homolog of the Drosophila gene diaphanous. *Science* **278**, 1315-1318.
Ma, E. Y. and Raible, D. W. (2009). Signaling pathways regulating zebrafish lateral line development. *Curr. Biol.* **19**, R381-R386.
Malicki, J., Avanesov, A., Li, J., Yuan, S. and Sun, Z. (2011). Analysis of cilia structure and function in zebrafish. *Methods Cell Biol.* **101**, 39-74.
Manor, U. and Kachar, B. (2008). Dynamic length regulation of sensory stereocilia. *Semin. Cell Dev. Biol.* **19**, 502-510.
McMahon, H. T. and Gallop, J. L. (2005). Membrane curvature and mechanisms of dynamic cell membrane remodelling. *Nature* **438**, 590-596.
Molla-Herman, A., Ghossoub, R., Blisnick, T., Meunier, A., Serres, C., Silbermann, F., Emmerson, C., Romeo, K., Bourdoncle, P., Schmitt, A. et al. (2010). The ciliary pocket: an endocytic membrane domain at the base of primary and motile cilia. *J. Cell Sci.* **123**, 1785-1795.
Nachury, M. V., Seeley, E. S. and Jin, H. (2010). Trafficking to the ciliary membrane: how to get across the periciliary diffusion barrier? *Annu. Rev. Cell Dev. Biol.* **26**, 59-87.
Perner, B., Englert, C. and Bollig, F. (2007). The Wilms tumor genes wt1a and wt1b control different steps during formation of the zebrafish pronephros. *Dev. Biol.* **309**, 87-96.
Perrin, B. J., Sonnemann, K. J. and Ervasti, J. M. (2010). β-actin and γ-actin are each dispensable for auditory hair cell development but required for Stereocilia maintenance. *PLoS Genet.* **6**, e1001158.
Peter, B. J., Kent, H. M., Mills, I. G., Vallis, Y., Butler, P. J. G., Evans, P. R. and McMahon, H. T. (2004). BAR domains as sensors of membrane curvature: the amphiphysin BAR structure. *Science* **303**, 495-499.
Qualmann, B. and Kelly, R. B. (2000). Syndapin isoforms participate in receptor-mediated endocytosis and actin organization. *J. Cell Biol.* **148**, 1047-1062.
Qualmann, B., Roos, J., DiGregorio, P. J. and Kelly, R. B. (1999). Syndapin I, a synaptic dynamin-binding protein that associates with the neural Wiskott-Aldrich syndrome protein. *Mol. Biol. Cell* **10**, 501-513.
Qualmann, B., Koch, D. and Kessels, M. M. (2011). Let's go bananas: revisiting the endocytic BAR code. *EMBO J.* **30**, 3501-3515.
Ravanelli, A. M. and Klingensmith, J. (2011). The actin nucleator Cordon-bleu is required for development of motile cilia in zebrafish. *Dev. Biol.* **350**, 101-111.
Sahly, I., Andermann, P. and Petit, C. (1999). The zebrafish eya1 gene and its expression pattern during embryogenesis. *Dev. Genes Evol.* **209**, 399-410.
Santos, F., MacDonald, G., Rubel, E. W. and Raible, D. W. (2006). Lateral line hair cell maturation is a determinant of aminoglycoside susceptibility in zebrafish (Danio rerio). *Hear. Res.* **213**, 25-33.
Schwintzer, L., Koch, N., Ahuja, R., Grimm, J., Kessels, M. M. and Qualmann, B. (2011). The functions of the actin nucleator Cobl in cellular morphogenesis critically depend on syndapin I. *EMBO J.* **30**, 3147-3159.
St Johnston, D. and Sanson, B. (2011). Epithelial polarity and morphogenesis. *Curr. Opin. Cell Biol.* **23**, 540-546.
Starr, C. J., Kappler, J. A., Chan, D. K., Kollmar, R. and Hudspeth, A. J. (2004). Mutation of the zebrafish choroideremia gene encoding Rab escort protein 1 devastates hair cells. *Proc. Natl. Acad. Sci. USA* **101**, 2572-2577.
Werner, M. E., Hwang, P., Huisman, F., Taborek, P., Yu, C. C. and Mitchell, B. J. (2011). Actin and microtubules drive differential aspects of planar cell polarity in multiciliated cells. *J. Cell Biol.* **195**, 19-26.
Westerfield, M. (1992) *The Zebrafish Book*.
Zigmond, S. H. (2004). Formin-induced nucleation of actin filaments. *Curr. Opin. Cell Biol.* **16**, 99-105.